Data-Driven Methods for the State of Charge Estimation of Lithium-Ion Batteries: An Overview

Panagiotis Eleftheriadis *[ID], Spyridon Giazitzis, Sonia Leva [ID] and Emanuele Ogliari [ID]

Department of Energy, Politecnico di Milano, Via Lambruschini 4, 20156 Milano, Italy;
spyridon.giazitzis@polimi.it (S.G.); sonia.leva@polimi.it (S.L.); emanuelegiovanni.ogliari@polimi.it (E.O.)
* Correspondence: panagiotis.eleftheriadis@polimi.it

Abstract: In recent years, there has been a noticeable shift towards electric mobility and an increasing emphasis on integrating renewable energy sources. Consequently, batteries and their management have been prominent in this context. A vital aspect of the BMS revolves around accurately determining the battery pack's SOC. Notably, the advent of advanced microcontrollers and the availability of extensive datasets have contributed to the growing popularity and practicality of data-driven methodologies. This study examines the developments in SOC estimation over the past half-decade, explicitly focusing on data-driven estimation techniques. It comprehensively assesses the performance of each algorithm, considering the type of battery and various operational conditions. Additionally, intricate details concerning the models' hyperparameters, including the number of layers, type of optimiser, and neuron, are provided for thorough examination. Most of the models analysed in the paper demonstrate strong performance, with both the MAE and RMSE for the estimation of SOC hovering around 2% or even lower.

Keywords: lithium batteries; estimation; data-driven; machine learning; state of charge

1. Introduction

Climate change has compelled humanity to seek alternative forms of energy production and reduce greenhouse gas emissions from hydrocarbon combustion. This has led to a shift towards renewable energy sources and the adoption of electric motors for electrifying transportation, which is considered a promising approach with numerous benefits [1]. Electric motors are powered by battery packs, making them a viable option. Wind turbines have emerged as a leading solution for renewable energy and are predicted to outpace fossil fuels by 2035, as reported by Forbes [2]. Unlike conventional steam generators that can be controlled by adjusting the fuel supply, renewable energy sources like wind and solar produce energy intermittently, necessitating immediate consumption or storage. This has led to the development of energy storage solutions, with LIB gaining significant popularity [3]. Currently, batteries dominate the field of energy storage, and some have reached their EOL status. This has given rise to the market for second-life battery products, which are used as alternatives to brand-new batteries [4].

Efficiently utilising batteries within a system requires detailed modelling to predict the battery's condition accurately. Two crucial aspects are the SOC [5] and the SOH [6], which provide valuable insights into the remaining energy, power delivery capacity, and overall cell life. Modelling batteries is complex and time-consuming due to their intricate electrochemical nature. Furthermore, the accurate assessment of the residual lithium in the battery presents a challenging task, demanding precise algorithms embedded within the BMS. These algorithms, based on mathematical models and/or machine learning techniques, are essential in estimating the battery's states, including SOC and SOH levels, using the information of the terminal voltage, terminal current, and surface temperature [5].

The SOC of a battery cell represents the capacity availability as a percentage of its maximum possible charge capacity [7]. Forecasting is not an easy undertaking [8] and

estimating the SOC is a challenging task, as it is a nonlinear function affected by various factors, including the voltage, current, temperature, and SOH [7], among others. Early attempts at accurate estimation involved two main techniques: open-circuit voltage-based methods [9] and CC [10]. However, these approaches were not able to accurately predict the SOC. To improve the accuracy, model-based methods were introduced, which combine an equivalent cell model with a suitable filter or observer. Commonly used filtering techniques include the Kalman filter [11], particle filter [12], H infinity filter [13], and observer-based techniques [14]. These methods rely on mathematical equations in estimating the SOC, but their computational cost is high.

Recently, the popularity and benefits of data-driven methods have surged, thanks to advancements in electronic materials and the vast amount of accessible data. On the other hand, model-based techniques, such as the equivalent circuit model, require the initial configuration of parameters [11]. Obtaining these parameters is challenging as they are dependent on the specific case and are influenced by the SOC, SOH, and temperature of the battery. Consequently, this process demands engineering expertise and experience, making it a laborious and complex procedure. On the contrary, data-driven methods have the advantage of not requiring extensive parameterisation and can effectively capture battery dynamics [15]. Several review articles have been published in recent years, but some of them lack a focus on data-driven techniques. For instance, in [16], the authors provide a comprehensive review of BMS implemented in electric vehicle applications to estimate the SOC, but without delving into data-driven methods or emphasising outdated articles. Similarly, ref. [17] presents a general review of electric vehicle-related issues but overlooks data-driven techniques. In another review [18], the authors cover the needs of electric vehicles and different techniques but lack a detailed analysis of data-driven approaches, which are currently outdated. In contrast, some articles have dedicated attention to data-driven methods. For example, in [19], the authors thoroughly analyse battery modelling and state estimation but lack more in-depth coverage of estimation techniques, especially data-driven ones. On the other hand, in [20], there is a complete review of SOC and SOH estimation using machine learning techniques, including theoretical explanations and comparisons between the methods reviewed. Similarly, in [15], the authors analytically explain the mathematical formulation of various data-driven techniques, estimation methods, testing procedures, and limitations. However, it lacks the inclusion of more recent articles on recurrent and deep learning combinations. A more recent article [19] focuses on SOC estimation trends but overlooks data-driven methods. Likewise, in [21], there is a comprehensive review of data-driven techniques but it does not cover many articles.

In light of the aforementioned gaps, this paper aims to present an overview of SOC estimation trends in the last five years, focusing on data-driven methods. Figure 1 depicts an overview of the included techniques. Building on the mathematical formulations covered in previous review articles, this paper focuses on the latest state-of-the-art articles published in the last three years. Each reviewed article was analysed considering the proposed algorithm, tested battery cell types, equipment, testing conditions, and their accuracy.

The screening process for this overview involved using the "Scopus" and "Google Scholar" databases, employing keywords such as SOC, machine learning, estimation, deep learning, and data-driven methods. More than 107 articles were identified over the last three years during the first screening, and they were assessed based on factors like the citation count, impact factor, and publication year. Subsequently, following the second screening process, 28 of these articles were selected in the same way for thorough review and analysis in this overview article. The main advantages and disadvantages of each method are presented in Table 1.
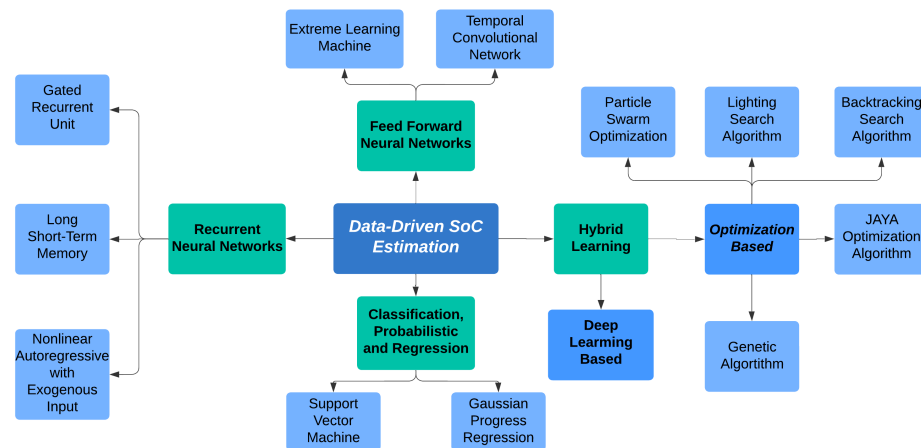
Figure 1. State-of-the-art data-driven techniques for estimation of the SOC.

Table 1. Advantages and disadvantages of each method.

Method	Advantages	Disadvantages
SVM	• Suitable for classification and regression tasks • Great accuracy for nonlinear and low-dimensional data	• Not recommended for handling large datasets due to its high computational demands • Difficult parameter selection • High complexity
GRP	• Suitable for classification and regression tasks • Capable of understanding and modelling complex, nonlinear connections within datasets • Incorporates prior information to improve predictions • Quickly identifies the maximum point of a function	• High computational cost • Complicated design of the appropriate kernel function • Poor scaling
DNN	• Applicable for many real-world applications (audio, text, image) • Can easily learn nonlinear and complex patterns • Great robustness • Fine-tuning flexibility	• Requires a large amount of data • High computational cost • Prone to overfitting • Optimal hyperparameter selection
TCN	• Cannot easily handle nonlinear and complex patterns • Complex calculation of the optimal hyperparameters (dilation rates, kernel size) • Limited long-term dependencies	• High computational cost • Complicated design of the appropriate kernel function • Poor scaling
LSTM	• Solves gradient-related issues • Captures long-term dependencies • Great robustness to noisy input data • Can learn complex and nonlinear patterns	• High computational cost • Hyperparameter sensitivity • Struggles with short-term patterns

Table 1. *Cont.*

Method	Advantages	Disadvantages
GRU	• Lower complexity than LSTM • Solves gradient-related issues • Less prone to overfitting and can be trained faster • Effective for shorter sequences	• Less effective for long sequences • Cannot easily capture complicated patterns • Sensitive to noisy data
Hybrid	• Enhanced performance • Feature extraction • Can be implemented in various tasks • Provides great robustness	• High computational cost • Complicated hyperparameter tuning • Prone to overfitting • Strong dependency on the weakest-performing component

This paper is organised as follows. In Section 2, we delve into classification, regression, and probabilistic techniques. Moving on to Section 3, we present feedforward neural network techniques. In Section 4, we focus on recurrent neural network techniques. Finally, in Section 5, we explore the hybrid learning approaches.

2. Classification, Regression, and Probabilistic

In this first section, data-driven methodologies will be discussed, incorporating classification, regression, and probabilistic approaches. Within this framework, the two principal categories are the SVM and the GPR, each offering distinct capabilities in solving the given problem. Despite their advantage of being suitable for use with small amounts of data, both techniques are facing declining popularity due to the significant increase in data volumes.

2.1. Support Vector Machine

An SVM is a data-driven method that is implemented for the classification and regression of linear and nonlinear data to detect outliers while improving the computational efficiency. The method is straightforward to implement and exhibits a strong capability to generalise with new data. Generally, the SVM algorithm searches for the optimal hyperplane that maximises the margin between the two classes. Moreover, when the data are not perfectly separable, the Soft-Margin SVM algorithm is used, which allows some misclassification. Furthermore, when the task is nonlinear and low-dimensional, it converts it into a linear and high-dimensional task by using the appropriate kernel function. Figure 2 demonstrates the linear and nonlinear classifier using the SVM algorithm. A detailed mathematical analysis of the SVM classifiers can be found in [22].
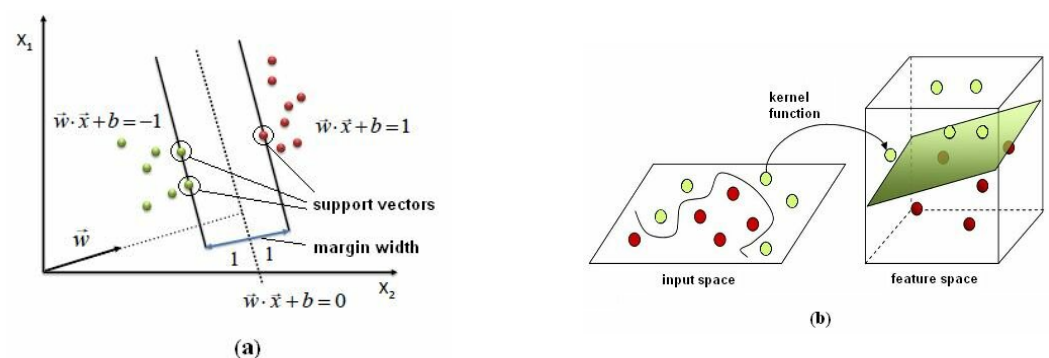

Figure 2. Linear and nonlinear SVM classifiers. (**a**) depicts a linear classifier, while (**b**) depicts a nonlinear classifier that transforms the original input space to a space with more dimensions named feature space [23].

In [24], an innovative framework is proposed for the joint estimation of the SOC and SOH by leveraging the strengths of two different models. Initially, the LS-SVM model is employed to extract degradation features from voltage and current data. These features are then used in conjunction with UPF, which incorporates a battery degradation model to optimise SOH estimation. Secondly, for the SOC estimation, an LS-SVM model is developed based on the correlation between the voltage and SOC. Then, the UPF is again employed, but, this time, it is adjusted by the SOH information using an ampere-hour integration model. The model is tested on a 2.2Ah NMC 18650 battery cell using a NEWARE BTS3000n battery cycler. The DST and capacity test are applied to generate the battery's dataset. The results demonstrate that the error of the SOC is below 2% over the battery's life cycle, and the RMSE of the SOH is under 4%. It appears that when the model utilises the SOH information, the accuracy, robustness, and stability increase. In this case, when noise is added to the SOH, the SOC error increases, although the results remain satisfactory. The proposed model, contrasted with the sample entropy model, provides superior results in estimating SOH while also requiring reduced computational effort, making it suitable for real-time applications. Moreover, it achieves better results than the EKF, DBN, and ECM-based models. The outcomes of the study are shown in Table 2. In general, the suggested model offers high accuracy and robustness. However, it should undergo testing across a broader range of temperatures and more complicated operational scenarios.

Although the SVM method can achieve satisfactory results, there are still many problems because it is a computationally expensive algorithm, can only be used in small datasets, there is difficulty in parameter selection, and when there is a multi-class task, the development of the optimal classifier is very complicated.

2.2. Gaussian Process Regression

GPR serves as a versatile tool utilised in classifying and regressing nonlinear data, as well as predicting time series with online learning capabilities. Moreover, it is frequently used when the task is to find the global maximum of a function as fast as possible, without considering the outputs. GPR begins by forming initial assumptions about the underlying function using a mean function and covariance function (kernel) in the prior stage. Subsequently, empirical observations play a key role in the next stage, leading GPR to revise these assumptions based on the data. This yields a posterior distribution that merges prior expectations and empirical insights, enhancing our understanding of the function and its uncertainty. The findings of the studies related to GPR are presented in Table 2. In [25], there is a comprehensive mathematical analysis of GPR. Figure 3 presents two smooth Gaussian processes, the Ornstein–Uhlenbeck and radial basis Functions, and includes both prior and posterior data. The dark line presents the current mean of the Gaussian process, while the grey lines are the samples. The black spots are the empirical observations, while the red triangle depicts the estimation of a new data point.

In [26], the authors developed a GPR model. Initially, an input set is prepared to correlate with the SOC using a strategy to extract the best features by analysing the correlation and computing the principal components of the input data. The simple GPR model achieves an RMSE of less than 3.4%, and in order to enhance its accuracy, an autoregressive GPR model is developed, resulting in an improved RMSE of less than 3%. Notably, the autoregressive GPR model proves to be effective in providing satisfactory estimations even under extreme conditions and when the initial SOC error is 20%. The battery pack, consisting of 177Ah NMC battery cells tested on a Digatron EVT 300–600 battery tester, achieves an impressive estimation error of less than 3.9%. Moreover, the model can achieve better accuracy and robustness by utilising the Pearson correlation coefficient than the Grey Relational Grade when the reduced matrix has fewer features. Furthermore, it has been observed that the sampling period's expansion shows a noticeable decrease in computation time. Additionally, the authors employed the DST and FUDS datasets to assess the model's alignment with aging and an initial SOC error within a margin of 20%. The model exhibited satisfactory performance and robustness even under some extreme conditions. Extending

testing to diverse temperatures and more intricate datasets is recommended to bolster the robustness assessment. Refining the hyperparameter selection process would also contribute to error reduction and overall model enhancement.
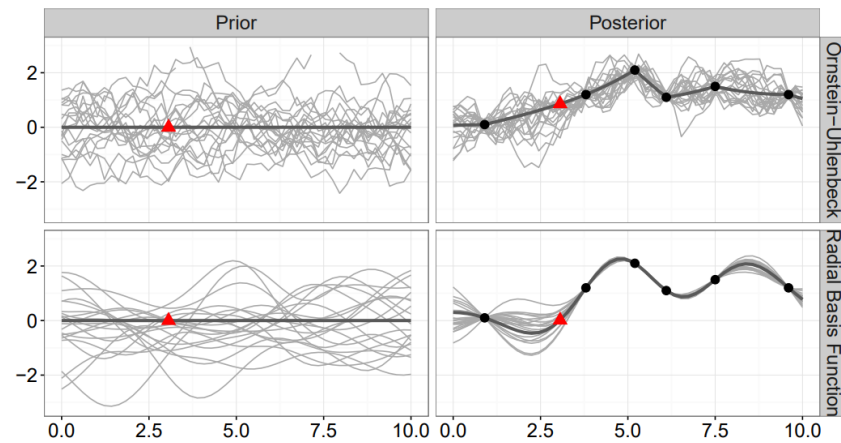

Figure 3. Gaussian processes that include prior and posterior data [25]. In this visual representation, grey lines represent data points generated by the Gaussian Process (GP), while black dots denote actual empirical observations. The dark grey line signifies the present mean estimate of the GP, and the red triangle represents the predictive outcome for the forthcoming data point.

In the paper by [27], a hybrid approach that integrates data-driven and model-based methods is introduced. Initially, the model utilises GPR to construct process and observation models derived from experimental datasets of batteries. Subsequently, the UKF model is implemented to boost the precision of SOC prediction by smoothing voltage deviations. Furthermore, the prediction model's mean and covariance functions are employed to depict the model's uncertainty. The proposed method was tested on two LFP battery cells, having different rated capacities, using the Arbin BT2000 battery tester. The accuracy of SOC estimation was evaluated across various health levels, spanning from the 50th to the 350th cycles. It was noted that the SOC estimation errors increased notably when the battery degradation reached higher levels. This increase in error is attributed to the reduction in the battery's total capacity, causing the real SOC value to be higher than the estimated value. Nonetheless, the overall model demonstrated exceptional accuracy, reliability, and generalisation capabilities for various testing conditions, with the maximum error remaining around 2%. For model validation, the utilisation of the UDDS and DST cycles is notable, given their capability to emulate diverse load profiles. However, their repetitive nature may lead the algorithm to rapid learning. Therefore, the inclusion of more intricate driving cycles is advised. These complex cycles could incorporate a randomised blend of diverse repetitive patterns, ensuring a rigorous assessment of the model's accuracy and better robustness.

The major drawbacks of this algorithm are the high computational cost when the dataset is large, the complicated construction of the right kernel, and the poor scaling. Generally, it achieves satisfactory results with low errors, but the high computational cost and complexity lead to large memory requirements. It also provides a solution for many real-world applications, such as image classification, text classification, and pattern recognition.

3. Feedforward Neural Network

The simplest structure of a neural network is the FFNN, where information always moves forward. FFNNs can have varying numbers of hidden layers, depending on the specific architecture and complexity of the network design. Still, in most cases, when referring to FFNNs, they refer to a "shallow" network consisting of one hidden layer, while those with multiple hidden layers are commonly known as "deep" networks (Figure 4). The term "deep learning" specifically emphasises the use of deep neural networks with

several hidden layers to extract hierarchical features from data. An FFNN operates by transmitting data across interlinked layers of nodes, with each layer modifying the input through weight and bias adjustments combined with activation functions before forwarding it to the subsequent layer. Through continuous parameter refinement during training, FFNNs can discern complex patterns and associations within data, rendering them valuable for applications such as image recognition and natural language processing. This type of NN is relatively straightforward and improves the computational and generalisation capabilities. The results of the studies related to FFNN algorithms are presented in Table 2.

In [28], an enhanced battery model was developed using an FFNN. Subsequently, the EKF algorithm was developed to create an FFNN-based SOC estimation method. Within this framework, an FFNN was employed to depict the battery's behavior, yielding the terminal voltage as its output. The model takes into account the battery current, surface temperature, SOC, and a novel parameter termed the "polarisation state of the battery" as its inputs. This unique polarisation state, distinct from the polarisation voltage, can only be computed using the cell's terminal current. Significantly, the polarisation state is well suited for datasets with variable sampling intervals, rendering its value independent of the interval size when the current remains constant. Careful consideration should be given to selecting the time constant in calculating the polarisation state, as it directly influences the model's complexity. The time constant value, ranging from 0 to 1000, is utilised alongside the correlation coefficient to assess the similarity among polarisation states, determined by a preset threshold. The robustness of this approach was tested on 2Ah lithium NCA 18650 battery cell data, examined at temperatures of $-10\,°C$, $0\,°C$, $10\,°C$, and $25\,°C$. To further validate the FFNN-based approach in real time, a hardware-in-loop (HiL) testbench was developed, featuring an actual battery, to closely emulate the operational conditions of electric vehicles. The findings demonstrate that after reaching a stable state, the errors in estimating the SOC can be maintained within a limit of 2%. The model was tested at various temperatures and with an error in the initial SOC and managed to provide satisfactory results (accuracy and robustness), even at very low temperatures. However, the model was only tested on the UNIF01 and MANHATAN datasets. The size and the complexity of the datasets are recommended to be increased to further test the performance of the model.

3.1. Deep Neural Network

Generally, DNN algorithms usually refer to multiple-layer FFNNs, and the way that they operate is mentioned above. Similarly, the model's efficiency can be determined from the number of hidden layers and neurons, while an optimiser can be used to fine-tune the hyperparameters, such as the number of hidden layers and neurons and the activation function, to name a few. Figure 4 depicts a DNN architecture consisting of an input layer with six inputs, five hidden layers with various numbers of neurons by each layer, and an output layer with two outputs.

Table 2. Summary of SVM, GPR, FFNN, DNN, and TCN techniques for SOC estimation.

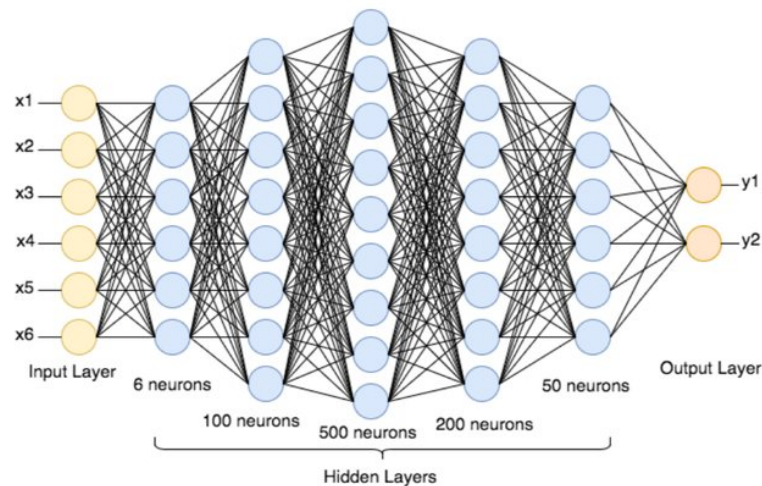| N/N	Ref	Algorithm	Battery	Temperatures	Performance
1	[24]	LS-SVM	2.2Ah NMC	25 °C	maxError 2%
2	[26]	GPR	177Ah NMC	25 °C and 0 °C	maxError 3.9%
3	[27]	GPR	2.55 and 2.6Ah LFP	10 °C and 40 °C	maxError 2%
4	[28]	FFNN	2Ah NCA	$-10\,°C$, 0 °C, 10 °C, and 25 °C	maxError 2%
5	[29]	DNN	2.9Ah NCA	20 °C, $-10\,°C$, 0 °C, 10 °C, and 25 °C	MAE 1.10% @ 25 °C, MAE 2.17% @ $-20\,°C$
6	[30]	TCN	2.9Ah NCA	0 °C, 10 °C and 25 °C	Average MAE 0.67% Average RMSE 0.87%

Figure 4. Deep neural network architecture [31].

In [29], the authors examined different DNN architectures for SOC estimation under constant and different ambient temperatures. For the constant ambient temperature case, the DNN comprised three layers with four, four, and one neuron(s) in each layer, respectively. However, in the case of a varying ambient temperature, the DNN consisted of four layers with 8, 16, 32, and 1 neuron(s) in each layer, respectively. The data collected from testing the 2.9Ah NCA 18650 battery cell using a Digatron battery tester at various temperatures ($-20\,^{\circ}\text{C}$, $-10\,^{\circ}\text{C}$, $0\,^{\circ}\text{C}$, $10\,^{\circ}\text{C}$, and $25\,^{\circ}\text{C}$) were utilised during the training phase of the DNN. After validation with multiple datasets, the DFNN achieved an MAE of 1.10% and 2.17% for the $25\,^{\circ}\text{C}$ and $-20\,^{\circ}\text{C}$ dataset, respectively. For the model evaluation, a wide variety of intricate driving cycles were employed, encompassing a significant range of temperatures. As the tests indicated, it was also robust to noisy data and measurement offsets. This method can be easily improved by optimising the hyperparameters using the grid search or Bayesian optimisation techniques.

To ensure satisfactory results, DNNs require a large amount of data, which can be difficult to acquire in many cases or can involve a time-consuming process. Furthermore, DNNs, particularly deep architectures, can exhibit computational intensity during both training and inference, resulting in high power consumption when implementing the model in hardware. Lastly, issues such as overfitting and hyperparameter tuning also need to be tackled.

3.2. Temporal Convolutional Network

A convolutional neural network is an enhanced type of artificial neural network that has gained widespread adoption in computer vision due to its sophisticated capabilities. While sharing the same architecture of input, hidden, and output layers with traditional ANNs, CNNs stand apart by employing a convolution operation in place of standard matrix multiplications between these layers. However, the TCN represents a specialised variant of the convolutional neural network especially designed for sequential data processing. TCNs employ a stack of convolutional layers to convolve input sequences with learnable kernels, capturing temporal patterns and dependencies. The introduction of dilation, which controls the kernel spacing, allows TCNs to efficiently model short- and long-term relationships in the data, addressing the exploding and disappearing gradient issue. This capability makes TCNs advantageous for tasks requiring the understanding of diverse time scales. TCNs offer parallelisability for faster training and inference compared to some recurrent models. Additionally, TCNs accommodate variable-length sequences through padding, maintain temporal equivariance, and exhibit robustness to input data time shifts, collectively establishing them as a versatile and effective option for diverse sequential data

analysis tasks. Figure 5 represents an architecture of a TCN with a kernel size of 5, with dilation of 1, 2, and 4, for input and hidden layers 1 and 2, respectively.
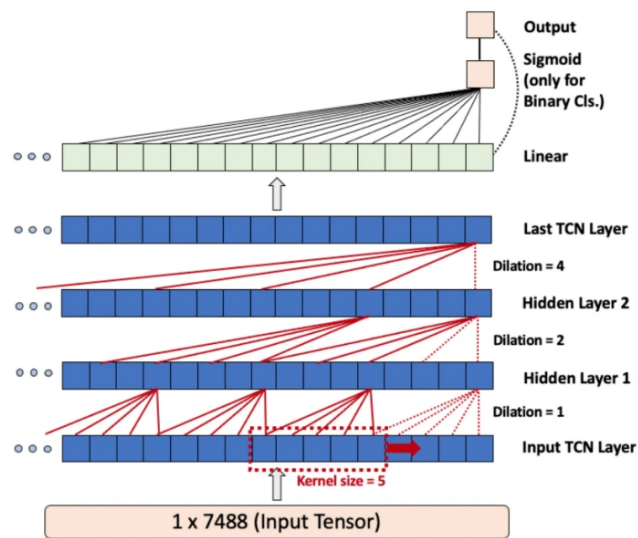

Figure 5. Temporal convolution network architecture [32].

In [30], a method using a TCN is proposed, where the TCN layer consists of six stacks, each containing four convolutional layers with a kernel size of 6, 64 filters, and dilation of 1, 2, 4, and 8 to learn input dependencies. The TCN can learn by itself and update its parameters according to the input data, leading to a model that accurately estimates the SOC under different conditions. The training process is sped up, and overfitting is prevented by employing an early stopping and declining learning rate strategy. During the training phase, the data were normalised to the range $[-1, 1]$, and the Adam optimiser was used to optimise the network parameters. This method was implemented in a 2.9Ah NCA 18650 battery cell under several testing conditions and achieved an average MAE and RMSE of 0.67% and of 0.87%, respectively. Using the transfer learning technique, the model can be applied to other types of LIB SOC estimation with minimal additional data for further training. A comparison test was also carried out between the TCN model and RNN methods, such as LSTM and GRU, which showed that the TCN model achieved more accurate results. The authors utilised a wide variety of complex datasets and varying temperatures to assess the model's accuracy. However, a robustness test was not conducted based on initial errors and noisy data. To enhance the model, the utilisation of a hyperparameter optimisation algorithm is recommended. Furthermore, in order to decrease the computational time of the model, the consideration of a compression method is advised.

In general, TCNs are capable of delivering precise estimation. However, they might face challenges in capturing long-term, complicated, and nonlinear relationships within the data. Another aspect to consider is the meticulous choice of hyperparameters, such as dilation rates, kernel size, and the number of layers, to ensure optimal performance.

4. Recurrent Neural Network

RNNs are specialised neural architectures for the processing of sequential data by maintaining internal states that capture previous information. They work iteratively, processing each sequence element while updating their hidden states, enabling them to model temporal dependencies. Crucial parameters to consider include the type of RNN architecture, the number of hidden units, the learning rate, and regularisation techniques. RNNs possess the advantage of handling variable-length sequences, making them suitable for tasks involving sequences of different lengths, such as natural language processing and time series analysis. However, they can face challenges related to vanishing gradients and capturing long-range dependencies. Despite these limitations, RNNs remain valuable in capturing temporal patterns in sequential data. This category includes the LSTM and GRU

NN, which can provide a solution to gradient-related problems. The outcomes of each study are summarised in Table 3.

4.1. Long Short-Term Memory Neural Network

The LSTM architecture is a type of RNN for sequential data processing that employs three gates (input, forget, and output) to regulate the information flow within the cell and successfully resolves vanishing and exploding gradient problems during backpropagation through time. The forget gate, influenced by the current input and previous hidden state, determines what to retain or discard from the cell state. The input gate, driven by the same inputs, decides which new information to incorporate. These gates influence the update of the cell state, which merges past and new information. Considering the input and hidden state, the output gate regulates which part of the cell state becomes the output. These mechanisms enable LSTMs to manage and leverage relevant information across sequential steps, facilitating the capture of intricate patterns in data. Figure 6 depicts the structure of an LSTM unit. Many LSTM units can be arranged in parallel and form an LSTM layer, where layers can be stacked and create a complex sequence deep learning model.

In [33], a method utilising LSTM-RNN is introduced, demonstrating strong generalisation capabilities in datasets for various conditions and temperatures. For this model, 10 driving cycles were created by using a random mix of the HWFET, UDDS, LA92, and US06 to be utilised for the training and testing phase of the proposed method. When tested on a 2.9Ah NCA 18650 battery cell using a Digatron battery tester at temperatures of 0 °C, 10 °C, and 25 °C, the method achieved a 0.573% and 1.606% MAE on datasets with steady temperatures and temperatures increasing from 10 °C to 25 °C, respectively. Furthermore, it was observed that augmenting the LSTM depth in time (from 250 to 1000) led to a progressively more accurate model. Ultimately, the proposed model has been shown to perform better with larger datasets and can yield satisfactory results even with incorrect initialisation. Despite the high accuracy of the model, the performance can be improved by optimising its hyperparameters.
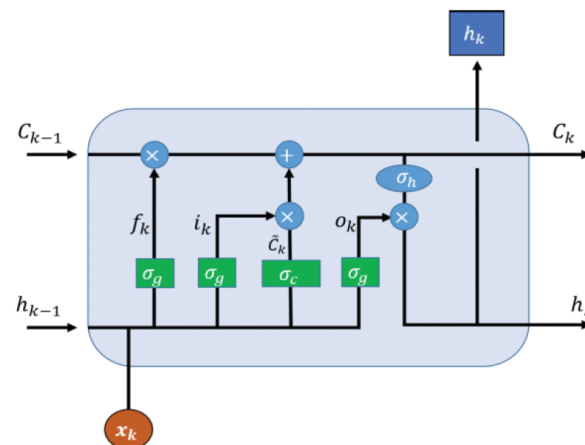
Figure 6. Structure of the LSTM unit [34].

In [34], a stacked LSTM network with three LSTM layers, each containing 50 nodes, is proposed. The same architecture was tested with 100 nodes per layer, but no significant improvement in performance was observed. A combination of the DST, US06, and FUDS datasets was used for the training and testing procedure. To prevent overfitting, a dropout layer with a rate of 50% was utilised for each LSTM layer. Testing was performed on 1.1Ah 18650 LFP battery cells using an Arbin BT2000 battery tester. Generally, the model achieved a 1.39% RMSE and 2.02% MAE. Moreover, to check the robustness of the model, incorrect initial values of the SOC were inserted. For these cases, the model's error remained under 2%, converging rapidly to the ground truth value of the SOC. Additionally, the proposed model demonstrated superior performance to the UKF. Additionally, it boasts a fast average

evaluation time, making it well suited for real-time applications. The model should be trained and tested in more complicated datasets and at more temperatures to provide satisfactory results in real-life conditions. Lastly, to improve its performance, hyperparameter optimisation is suggested.

In [35], the authors proposed a combined data-driven and model-based method. Firstly, a one-layer LSTM model with 32 units was employed to estimate the SOC, using the Coulomb counting method to generate the ground truth value of the SOC. The estimated SOC was obtained by implementing an ACKF. The LSTM model takes input with a sequence length of 30 in the time series. The Adam optimiser was employed, and the value of epochs for the validation datasets was set to 75. Utilising the information from CALCE [36] of a 2.23Ah 18650 LFP, the model achieved an RMSE below 2.2% and an MAE under 4%. Even when the initial SOC value has an error of 40%, the proposed method provides satisfactory SOC estimations and converges quickly. This makes the model well suited for real-time applications with uncertainty and noise. Notably, this model performed better than the simple LSTM and the hybrid LSTM with the Cubature Kalman Filter models. The authors employed a trial-and-error approach to tune the hyperparameters, which was both time-consuming and prone to yielding significant errors. This challenge can be mitigated by adopting a hyperparameter optimisation algorithm. Furthermore, the datasets utilised for the training and testing of the model were relatively simple, necessitating the incorporation of more complex datasets.

Similarly, in [37], a one-layer LSTM with 300 nodes was proposed to estimate the battery SOC, incorporating a UKF to filter the noise and minimise estimation errors. The Adam optimiser was implemented, with a 0.01 learning rate, while the data were normalised to the range $(-1,1)$ using min-max normalisation. Testing was conducted on 1.1Ah 18650 LFP cells at temperatures of 0 °C, 10 °C, 20 °C, 30 °C, and 40 °C. The RMSE and MAE were below 1.1%, surpassing the performance of other models such as SVM, GPR, and other NNs. Additionally, when the proposed model was tested with temperatures that had not been included in the training phase, it achieved satisfying results, as well as when the authors considered an erroneous initial value of the SOC. For network parameter determination, the trial-and-error method was used, which is computationally costly and, in most cases, is not optimal. By applying a hyperparameter optimisation algorithm, this challenge can be easily solved. Moreover, the training and testing datasets were relatively basic, prompting the consideration of more complex datasets for a comprehensive evaluation.

The authors in [38] present a fresh approach to estimating the charging status of two lithium-ion batteries. This method employs an LSTM model with an attention mechanism to achieve accurate and efficient predictions. The proposed model comprises two hidden layers, the LSTM and the attention mechanism, which are designed to predict the final SOC and incorporate long-term dependencies by placing the attention mechanism in the output layer of each LSTM unit. To ensure robustness, the Monte Carlo dropout technique is utilised. The datasets used for evaluation consist of a 2Ah 18650 NMC cell acquired from CALCE [36] and a 2.9Ah Panasonic NCA cell obtained from the University of Wisconsin–Madison [39]. The model attains better performance by incorporating additional training datasets, while the input length is 76. Throughout all experiments, the RMSE obtained from the proposed model remains below 1.41%, outperforming the basic LSTM and bidirectional LSTM models. Nevertheless, hyperparameter optimisation is recommended to be used to improve the model accuracy and to ensure robustness; introducing initial errors into the data should be explored further.

In [40], a novel architecture was developed incorporating stack bidirectional LSTM neural networks, enabling the model to capture intricate dependencies within the input data effectively. For the model's validation, the datasets from the University of Wisconsin–Madison [39] and CALCE [36] were employed, referring to a 2.9Ah 18650 NCA and a 2Ah 18650 NMC battery cell, respectively. The model proposed in the study, comprising two bidirectional LSTM layers, each consisting of 64 hidden neurons, demonstrates remarkable performance, achieving MAEs as low as 0.46% and 0.73% for standard and fluctuating

temperatures, respectively. Several techniques were employed during the training process to augment the model's efficacy. Firstly, the input data were normalised within the range of (0, 1) to facilitate more efficient convergence. Secondly, the ReLU activation function was implemented in the output layer, contributing to enhanced nonlinearity and expressiveness in the predictions. Thirdly, the Adam optimiser, utilising default settings, was chosen to optimise the model's parameters, ensuring better convergence and faster training. Furthermore, the training was conducted for 5000 epochs to learn intricate patterns within the data thoroughly. Lastly, a dropout layer was incorporated with a masking probability of 20%, promoting regularisation and mitigating overfitting, thereby improving the model's generalisation ability. In conclusion, the stacked bidirectional LSTM performs better than the recurrent SRNN, GRU, and LSTM models. Moreover, it can estimate the SOC for various battery types across different temperatures, delivering satisfactory estimations. Despite the authors' extensive use of complex datasets for the testing and training of the model, the assessment of its robustness remains inadequate. Furthermore, the absence of a hyperparameter optimisation technique is notable; instead, the authors relied on a trial-and-error approach to determine the optimal values. This method is not only time-consuming but also can provide inaccurate results.

In [41], an encoder–decoder architecture based on bidirectional LSTM is proposed for SOC estimation under various testing conditions. The study utilised the dataset from the University of Wisconsin–Madison [39], which pertained to a 2.9 Ah 18650 NCA battery cell, to examine the proposed model. The Adam optimiser with default settings and a dropout masking probability of 20% were utilised. Data were normalised to the range [0, 1], and the model was trained for 5000 epochs. The proposed approach achieved an impressive 1.07% MAE across different temperatures, effectively learning complex dependencies from both directions to enhance the learning of temporal information. The selection of an optimal configuration involved trial-and-error experimentation, which led to a sequence length of 40, two bidirectional LSTM layers, and 64 bidirectional LSTM units. Notably, when the sequence length is too short, it fails to comprehend the internal attributes of the LIB, while excessively long sequences might hinder the effective capture of temporal dependencies. Satisfactory estimates can be obtained even with varying ambient temperatures. Moreover, several tests were conducted to find the optimal sequence length, width (biLSTM units), and depth (biLSTM layers) for different temperatures, namely 40, 64, and 2, respectively. The authors employed a trial-and-error approach to determine the optimal hyperparameters for the model, including factors such as the BiLSTM units and sequence length, instead of utilising a hyperparameter optimisation algorithm, which is a time-consuming method and can lead to unsatisfactory results. Furthermore, the study did not involve the introduction of initial errors in the input data to assess the model's robustness.

Despite their significant advantages, LSTM neural networks also entail several drawbacks compared to other data-driven methods. LSTMs' complex architectures can render them computationally demanding, resulting in long training periods and high memory requirements. Although LSTMs excel in capturing long-term dependencies, they might encounter challenges in recognising specific short-term patterns within data. Furthermore, determining the most suitable LSTM architecture and optimal hyperparameters can necessitate extensive experimentation or the adoption of hyperparameter optimisation techniques, which are highly time-consuming.

4.2. Gated Recurrent Unit Neural Network

The GRU architecture is a more basic variant of the LSTM model, featuring two gates: the reset and update gates. The reset gate controls the extent to which previous information is incorporated into the current hidden state, enabling the model to discard or retain past information adaptively. The update gate, conversely, determines the degree of influence that the current input and the previous hidden state have on the updated hidden state. GRUs are characterised by a more straightforward internal structure than LSTMs, resulting in decreased computational complexity. During data flow, the GRU takes input data and

computes the reset and update gate activations, updating the hidden state by blending the reset and current input. This updated hidden state influences the final output, making the GRU computationally efficient and effective in modelling sequential data. Figure 7 presents the structure of a GRU unit, which can form a GRU layer and, by stacking layers, can compose a complex model.
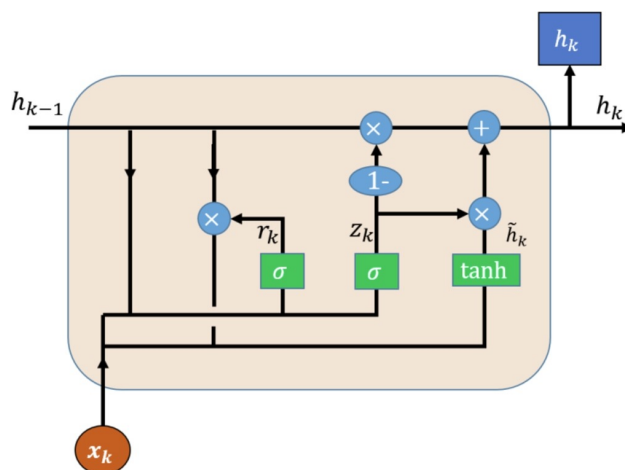

Figure 7. Structure of the GRU unit [42].

In [42], a GRU model is proposed for the estimation of the SOC. The framework comprises the input layer, the GRU layer with 150 nodes, the FC layer with 80 neurons, and the output layer. The model demonstrates robustness when the initial SOC is uncertain and achieves great performance when it is trained on various temperatures, with an input sequence length of 30. The proposed method is tested on two battery cells, the 1.3Ah 18650 NMC and the 1.1Ah LFP, in various temperatures (0 °C, 10 °C, 20 °C, 30 °C, 40 °C, and 50 °C). The results indicate that the model precisely estimates the SOC at different temperatures, achieving a 3.5% RMSE, even when predicting over unknown temperature conditions. This paper proves that LFP batteries require more hidden neurons compared to the NMC battery in capturing the complicated properties of the battery due to the presence of a plateau in the OCV–SOC curve. In the case of the NMC battery, the model consistently maintained RMSEs below 2.5%. The US06 and FUDS datasets were used to test the proposed model, while the DST dataset was utilised for the training process. These datasets tend to have repetitive patterns, which are not present in real-world applications. Moreover, a hyperparameter tuning algorithm should be employed to improve the model's accuracy.

In [43], a GRU-RNN method is presented, comprising an input layer with three nodes, a GRU layer with 1000 nodes, an FC layer with 50 nodes, and an output layer with one node. The model was trained using an Adam optimiser with a learning rate of 0.0001. Evaluating input sequences of 250, 500, and 1000, it was found that a sequence length of 1000 resulted in superior performance. For the model evaluation, two battery datasets, 2Ah 18650 NCA and NMC, were acquired from McMaster in Canada [29] and from CALCE [36], respectively. Additionally, an 18Ah battery cell dataset was examined using high C-rate pulses to discharge the battery cell at three different temperatures (0 °C, 10 °C, and 25 °C). This model demonstrates its capability in accurately estimating the SOC under varying temperatures, reaching 0.86%, 1.75%, and 1.05% MAEs, for the aforementioned datasets, respectively. Research on the influence of the hyperparameters, such as the time step, iterations, and training data size, shows that increasing these hyperparameters enhances the accuracy of the GRU model. The experimental setup involved configuring the time step, iteration, and mini-batches to 1000, 100, and 72, respectively. Before processing, the data underwent normalisation, resulting in a range between 1 and 1. The input features comprised time series data of the voltage, current, and temperature, with varying lengths explored between 250, 500, and 1000. Interestingly, the investigation revealed that the most favourable sequence length for the input data was 1000 s. Subsequent comparison tests

demonstrated that the proposed GRU-RNN model outperformed a standard RNN model. Furthermore, it must be noted that the GRU model yielded accurate estimations of the SOC, even when confronted with mixed charge and discharge data and high C-rate discharge pulses. However, for a more comprehensive evaluation of the model's robustness, it is essential to conduct thorough tests using noisy data and introducing initial errors. In conclusion, for improved accuracy, expanding the model's training across various temperatures and implementing a hyperparameter tuning algorithm are recommended procedures.

In [44], another GRU method was proposed, consisting of a one-layer GRU with 30 nodes. This model uses voltage and current measurements to predict the SOC through the GRU-RNN's output. The momentum gradient algorithm optimises the network weights by considering both the gradient direction and the previous values of the current example, effectively preventing weight change oscillations and improving the convergence speed. Noise is added to the sample data to mitigate overfitting and enhance generalisation capability. The data preprocessing step involves using min-max normalisation, while the model was trained under different momentum terms β, noise variance σ, and numbers of hidden layer neurons. The method was tested under various operation conditions using a 2.2Ah LIB on a NEWARE CT-4008TB battery tester. In the first analysis, increasing β from 0 to 0.6 accelerated the error reduction and reduced oscillations, but β equal to 0.8 caused noticeable oscillations. In general, a proper β leads to smaller SOC errors. Furthermore, for varying noise variances, the smallest RMSE and MAE were found for σ equal to, while, as σ increases, the RMSE and MAE rise. The model obtained the smallest RMSE and MAE values by using 30 hidden neurons. This model achieved a 1.52% and 1% RMSE and MAE, respectively, while the model's performance can be further enhanced by increasing the hidden layer's neurons. Determining the ideal number of hidden layers and neurons can be achieved through a hyperparameter tuning algorithm. Furthermore, the model's performance evaluation relied on a relatively simple dataset, indicating the importance of integrating more complex datasets to evaluate its performance better. Additionally, expanding the input features beyond the voltage and current could substantially improve the accuracy of the model. For instance, temperature information can significantly influence the accurate estimation of the SOC in battery systems.

In [45], the authors proposed a GRU model that utilises an altogether method to optimise the model, utilising optimisers like Nadam and AdaMax to learn its own parameters rapidly. During the model's pre-training phase, the Nadam optimiser is obtained to swiftly locate the minimum optimised value. Subsequently, the AdaMax optimiser is employed to refine the model parameters in the fine-tuning phase. The evaluation dataset consisted of data from a 2.3Ah 26650 LFP battery cell, which were sourced from CALCE [36]. The proposed GRU model comprises an input layer, a GRU layer with 260 units, an FC layer, and an output layer. To prevent overfitting, the dropout method was applied using a masking probability of 20%. The batch size was set to 230 and the epochs to 100, while min-max normalisation was implemented to scale the data. This method demonstrates remarkable performance, achieving an impressive 1.13% RMSE and an 0.84% MAE, while effectively reducing the training time of the model and enhancing its performance. Additionally, the ensemble optimiser surpasses the Adam optimiser and the GRU-Ensemble and showcases superior performance, exhibiting a lower error than the LSTM-Ensemble. Nonetheless, the testing and training datasets employed for the model were relatively simple, lacking initial errors and offsets essential for robustness assessment. Moreover, using algorithms like grid search or Bayesian optimisation could have been beneficial to determine optimal hyperparameter values, thereby enhancing the model's overall performance.

Table 3. Summary of RNN techniques for SOC estimation.

N/N	Ref	Algorithm	Battery	Temperatures	Performance
1	[33]	LSTM	2.9Ah NCA	0 °C, 10 °C, and 25 °C	MAE 0.573% @ fixed T MAE 1.606% T: 10 to 25 °C
2	[34]	Stacked LSTM	1.1Ah LFP	25 °C	RMSE 1.39%, MAE 2.02% inaccurate initial SOCs: RMSE 2%, MAE 1%
3	[35]	LSTM	2.23Ah LFP [36]	Yes	RMSE 2.2%, maxError 4%
4	[37]	LSTM	1.1Ah LFP	0 °C, 10 °C, 20 °C, 30 °C, and 40 °C	RMSE 1.1%, MAE 1%
5	[38]	LSTM with Attention	2.9Ah NCA [39], and 2Ah NMC [36]	Yes	RMSE 1.41%
6	[40]	Stacked biLSTM	2.9Ah NCA [39] and 2Ah NMC	Yes	MAEs 0.46%, 0.73% @ fixed and varying temperature
7	[41]	biLSTM (ED based)	2.9Ah NCA [39]	Yes	MAE 1.07% @ varying T
8	[42]	GRU	1.3Ah NMC, 1.1Ah LFP	0 °C, 10 °C, 20 °C, 30 °C, 40 °C, and 50 °C	RMSEs 2.5% NMC, 3.5% LFP
9	[43]	GRU	2.9Ah NCA [29], 2Ah NMC [36] and 18Ah new	0 °C, 10 °C, and 25 °C	MAEs 0.86%, 1.75%, 1.05%, resp.
10	[44]	GRU	2.2Ah	-	RMSE 1.52%, MAE 1%
11	[45]	GRU	2.3Ah LFP	0 °C, 30 °C, and 50 °C	RMSE 1.13%, MAE 0.84%

The main disadvantage of the GRU-NN is its potential limitation in capturing intricate long-term dependencies in data compared to more complex architectures like the LSTM. Additionally, due to their simpler design with fewer gating mechanisms, GRUs are more prone to overfitting, as they struggle to generalise to complex data patterns and are more sensitive to noise present in the training data.

5. Hybrid Learning Approach

The combination of data-driven techniques has become a subject of considerable interest, aimed at elevating the overall performance of SOC estimation models. This fusion is classified into optimisation and deep-learning-based models. By synergistically harnessing the strengths of these two categories, SOC estimation techniques stand to achieve notable advancements in their overall effectiveness and applicability across a wide range of practical scenarios.

5.1. Optimisation-Based Algorithm

Optimisation-based algorithms often integrate a neural network model to establish initial values, which are then fine-tuned through an optimisation algorithm to optimise the hyperparameters. The primary objective of these algorithms is to enhance convergence by overcoming challenges associated with local minimum values within non-convex functions. By iteratively adjusting the parameters and optimising the hyperparameters, these methods facilitate more efficient and effective optimisation, yielding improved performance and enhanced convergence properties in the overall optimisation process. Some examples of such algorithms include BSA, GSA, PSO, JAYA optimisation, LSA, and GA, and the results of each are shown in Table 4.

In [46], a model was developed by combining the ELM algorithm with GSA to determine the number of neurons at the hidden layer. The ELM architecture consisted of 3 layers—input, hidden, and output. For GSA, the population size was set at 50, while the iteration number was 100, with the constraint for hidden layer neurons ranging from 0 to 500. The optimal number of hidden layers for different datasets and temperatures was

determined. The improved ELM algorithm showed superior generalisation performance at various operating conditions and achieved a low computational cost of under 0.6 s. The data were split into 70% for training and 30% for testing and normalised to a range of (−1, 1). The method, tested on an NMC 18650 battery cell at different temperatures, achieved an RMSE of 1% and 1.6% for different datasets, outperforming other algorithms. Finally, the proposed model demonstrated accurate SOC estimates even when subjected to Gaussian noise, utilising a moving average filter. By using the GSA for the hyperparameter tuning, the proposed method demonstrated advanced flexibility in adapting to different datasets, without setting a large and flexible hyperspace.

In [47], a backpropagation neural network with three feedforward layers was enhanced using a BSA to find the most suitable hyperparameters. The BSA used a population size of 100, a mix rate of 0.9, and a two-dimensional search space. The approach employed data from a 2Ah 18650 NMC battery obtained from CALCE [36]. The authors used 70% and 30% of the overall data to train and test their model. In addition, an average filter was applied to the data to reduce noise, and then the data were normalised to a range of (−1,1). The outcomes of the BSA were showcased for both dynamic profiles, namely DST and FUDS, across three distinct temperatures, 0 °C, 25 °C, and 45 °C. At 0 °C, the method attained an RMSE of 1.47% and an MAE of 0.76%. Moreover, a comprehensive performance evaluation was performed, comparing the proposed BPNN-BSA model with other existing models like RBFNN-BSA, GRNN-BSA, and ELM-BSA. The analysis demonstrated that the BPNN-BSA model exhibited superior accuracy and robustness compared to the other models, particularly when subjected to diverse temperature conditions and electric vehicle profiles. Utilising the BSA algorithm for hyperparameter tuning, the suggested technique showcased commendable flexibility in acclimating to a single dataset. However, the authors missed an opportunity to comprehensively assess the proposed method's effectiveness by not conducting tests across a broader range of datasets.

In [48], a hybrid model is presented, comprising a DBN with a KF to estimate the SOC, with the whole model's parameters optimised using a PSO algorithm. The DBN architecture consists of two layers: a logistic regression and a stacked restricted Boltzmann machine with visible and hidden layers. The amount of hidden neurons is determined by the RBM's parameters. This model is tested using a 2.2Ah NMC battery cell tested under various conditions and a randomly generated battery dataset from NASA PCoE [49]. This approach yields an MAE under 2.2%, with an RMSE below 0.7% and MAE below 0.57% for DST profiles, outperforming the simple DBN. In this research, a series of comprehensive tests were conducted, highlighting the superior performance of the DBN-KF model compared to DBN. In particular, the DBN-KF model exhibited enhanced estimation accuracy for the SOC under dynamic conditions. Furthermore, the investigation revealed that possessing information about the initial SOC value significantly accelerated the overall convergence time. Through the utilisation of the PSO algorithm for hyperparameter tuning, the presented approach demonstrated enhanced versatility in its capacity to conform to diverse datasets. Nevertheless, it is important to acknowledge that the straightforwardness of the proposed model might lead to more pronounced errors in practical real-world applications.

In [50], a novel approach is introduced, which involves an efficient type of neural network. The method approximates the discrete nonlinear and dynamic system using a polynomial NARX model. The input variables of the neural network are normalised and selected using the fast-forward input selection algorithm. The JAYA optimisation scheme is employed to fine-tune the essential parameters of the RBFNN. The parameters of the NARX model are set through the application of a trial-and-error method. The method is evaluated using 216 LFP battery cells with serial connection, achieving a 0.3172% RMSE and 0.1926% MAE. The optimised model significantly reduces the RMSE and MAE errors compared to the RBF model without optimisation. Through the application of the JAYA algorithm for hyperparameter tuning, the proposed technique displayed an elevated capacity for generalisation in its adaptation to a singular dataset. Despite the dataset's extensive cell count, the authors missed an opportunity to enhance the study's credibility by

incorporating a different dataset to evaluate the framework's efficacy. Notably, the proposed method optimises its input selection using the fast-forward selection algorithm, exclusively employing the most relevant features for SOC prediction.

Table 4. Summary of optimisation-based hybrid techniques for SOC estimation.

N/N	Ref	Algorithm	Battery	Temperatures	Performance
1	[46]	ELM + GSA	NMC	25 °C and 45 °C	RMSE 1.1% DST, 1.4% FUDS and 1.8% US06
2	[47]	BPNN + BSA	2Ah NMC [36]	0 °C, 10 °C, and 25 °C	RMSE 1.74%, MAE 0.87% @ 0 °C
3	[48]	DBN + PSO	2.2Ah NMC [49]	Yes	AvgError 2.2%, DST: RMSE 2.2%, MAE 0.57%
4	[50]	NARX + RBFNN + JAYA	LFP	Yes	RMSE 0.3172, MAE 0.1926
5	[51]	RNARX-NN + LSA	3.2Ah NCA, [36]	0 °C, 25 °C and 40 °C	RMSE 0.8937%
6	[52]	NARX-NN + LSA	2Ah NMC [36]	0 °C, 25 °C, and 45 °C	RMSE 1.26%, MAE 0.76% @ 0 °C
7	[53]	SGAGM	2.6Ah LC	Yes	MAE less 1%

In [51], a novel RNARX neural network algorithm is proposed, which benefits from the computational capabilities of LSA to identify optimal hyperparameter values. The RNARX method is structured with an input, hidden, and output layer, incorporating feedback loops. The model's hidden and output layers employ transfer functions, such as logsig and purelin, respectively, to carry out specific operations. Data were randomly split in a 70 to 30 ratio, to create the training and testing groups, and then were normalised to a range of (−1, 1). To evaluate the method, a 3.2Ah NCA battery cell was tested using a NEWARE BTS-4000 at temperatures of 0 °C, 25 °C, and 40 °C. The values for input delay, feedback delay, and the number of hidden neurons were determined as 2, 4, and 7, respectively, resulting in an RMSE of 0.8937%. Additionally, dynamic drive cycle data from CALCE [36] were utilised for the validation of the method. The study further explored the effects of aging and noise, showing that the proposed model yielded satisfactory results even under these challenging conditions. The study included a comprehensive comparison test, evaluating the proposed RNARX-LSA model against the BPNN, ELM, RBFNN, DRNN, and RF algorithms. The results clearly indicated that the RNARX-LSA outperformed all other methods in terms of SOC estimation accuracy. Furthermore, the RNARX-LSA method demonstrated a significantly smaller SOC error when compared to other approaches for hyperparameter tuning, such as the RNARX-BSA, RNARX-PSO, and RNARX-GSA methods. This underscores the exceptional performance and efficacy of the RNARX-LSA method in estimating the SOC. Applying LSA for hyperparameter tuning, the presented technique demonstrated heightened flexibility concerning the employed datasets. However, it is worth noting that the authors could have enhanced the study by testing the method across a broader array of datasets and expanding the hyperspace with additional hyperparameter options. Conversely, the comprehensive examination of factors like aging effects and noise contributes to positioning the proposed framework as a holistic solution, verified through trials in quasi-real-world scenarios.

The paper by [52] introduces an enhanced NARX-based neural network algorithm, which utilises the LSA technique to determine optimal values for input delays, feedback delays, and the number of hidden layer neurons. The LSA findings are demonstrated for the FUDS and US06 dynamic profiles at three different temperatures: 0 °C, 25 °C, and 45 °C. An optimisation process is performed to identify the best configurations for hidden layers, input delay, and feedback delay. The optimal values for the three temperatures are found to be 3, 7, and 3 for 0 °C; 3, 6, and 2 for 25 °C; and 11, 9, and 16 for 45 °C. The LSA

parameters, such as the population size and iterations, are set to 50 and 100, respectively, with a maximum value of 10 for the channel time. The limit range for hidden nodes is set from 0 to 20, while the limit range for input and feedback delays is set from 1 to 10. Transfer functions such as tansig and purelin are applied in the hidden and output layers, respectively. To evaluate the method, data from a 2Ah 18650 NMC battery acquired from CALCE [36] are used, achieving an RMSE of 1.26% and MAE of 0.76% at 0 °C. The SOC value for each lithium-ion cell is calculated as the average value of the battery pack's SOC. Additionally, for the monitoring and balancing of the voltage of the battery pack, a charge equalisation method is utilised. Comparative tests show that LSA outperforms PSO in terms of objective function values, and the NARXNN-LSA method demonstrates superior performance in terms of lower errors and computation time compared to the BPNN-LSA and RBFNN-LSA algorithms. Similarly to the prior approach, employing LSA for hyperparameter tuning revealed the proposed method's heightened adaptability to the utilised dataset. Moreover, this study encountered the same limitation of constrained generalisation due to relying solely on a single dataset and exploring a narrow range of hyperparameters.

The paper by [53] presents a novel estimation approach called SGAGM, which combines GM with GA to estimate the SOC of batteries. The SGAGM(M, m, N) algorithm is utilised for SOC estimation, where M, m, and N represent the window size, sliding data, and predicted data, respectively, with values set to 8, 1, and 1. Two datasets were used to validate this method. The first dataset consisted of a 2Ah 18650 battery cell acquired from NASA's dataset [54], while the second dataset was of a 2.6Ah LCO battery cell tested on an ITECH electronic load IT8511A+. The SGAGM method achieved an impressive MAE of less than 1% and a maximum error of less than 1.04%, demonstrating its high accuracy in SOC estimation under different temperatures and working conditions. Furthermore, the SGAGM method outperformed the GM(1,1) method in terms of estimation accuracy. Through the utilisation of GA for hyperparameter tuning, the suggested approach showcased commendable generalisation capabilities across both employed datasets. These datasets encompassed both publicly available data and data derived from their proprietary experimental setup. Nonetheless, a shortcoming of the study pertains to the limited scope of the hyperparameters explored within the model, potentially leading to the suboptimal performance of the framework.

5.2. Deep Learning

Deep-learning-based models possess a distinct advantage in merging diverse data-driven models and concatenating them to construct larger and more sophisticated networks. This characteristic enables these models to exhibit enhanced performance when tasked with handling a wide array of complex and diverse challenges, encompassing tasks related to feature extraction and prediction. By seamlessly combining multiple models, like FFNNs, CNNs, and RNNs, to name but a few, and leveraging the power of deep neural networks, deep learning approaches showcase remarkable adaptability and capability in effectively addressing intricate problems in various domains. The corresponding outcomes of each relevant research article are presented in Table 5. An inherent limitation in the following approaches is the absence of proper hyperparameter tuning. In these cases, the hyperparameters for the subsequent models are primarily adjusted using trial-and-error techniques.

In [55], a combined CNN-LSTM network is proposed, where the CNN is responsible for extracting advanced spatial features from battery parameters, and the LSTM models the relationships among the present and the former inputs to capture temporal features. The CNN architecture consists of three convolutional layers, each consisting of six filters to extract spatial features, and the size of each hidden layer matches the input layer's size. The LSTM layer contains 300 hidden nodes to learn the temporal features, and an FC layer with 80 nodes is utilised for SOC estimation. Evaluating a 1.1Ah LFP 18650 cell on an Arbin BT2000 at temperatures ranging from 0 °C to 50 °C, the model attains a maximum

MAE under 1% and a maximum RMSE less than 2%. This method outperforms the simple CNN and LSTM methods in accurately mapping the impact of temperature, achieving an MAE below 1.5% and RMSE below 2% even under various temperatures. It was noticed that the RMSE and MAE values were slightly higher in the 40–80% SOC range due to the plateau area in the SOC–OCV curve, where small voltage errors significantly affected the SOC estimation. The study also suggests updating the network parameters to account for battery aging effects. By combining a CNN to extract spatial features and LSTM to enhance the capture of temporal features, the framework gains a generalisation capability. However, the study's scope was limited to a single dataset, omitting the exploration of various datasets that would typically be expected.

In [56], a hybrid data-driven method using a dynamic NARX model combined with LSTM-RNN is presented, addressing the issues of gradient explosion and gradient descent. The NARX model uses current, voltage, and temperature inputs to predict the SOC, and the predicted SOC, along with the same inputs, is subsequently fed into the LSTM network. Both networks have 70 hidden layers, with input and feedback delays set at 1:2. The 'trainlm' function is employed for training, and 3000 samples of initial current, voltage, and SOC estimations are used as input to train the LSTM model. Testing on an LFP 18650 battery cell using an EVT500-500 battery tester, the proposed method achieves an RMSE below 1% and exhibits high multi-time prediction performance, surpassing the BPNN-PSO, LSTM, and LL-SVM models. Overall, the proposed model achieves a significant 60% improvement over the classic LSTM model. Employing the NARX model as the initial predictive layer and utilising its output as input for the LSTM network, this approach establishes a two-step prediction solution with remarkable accuracy. However, the framework's applicability is hindered by relying solely on a single dataset, constraining its potential for broader generalisation.

Table 5. Summary of deep-learning-based hybrid techniques for SOC estimation.

N/N	Ref	Algorithm	Battery	Temperatures	Performance
23	[55]	CNN + LSTM	1.1Ah LFP	0 °C, 10 °C, 20 °C, 30 °C, 40 °C and 50 °C	maxMAE 1%, maxRMSE 2% and maxMAE 1.5%, maxRMSE 2% @ varying temp.
24	[56]	NARX-NN + LSTM	LFP	No	RMSE 1%
25	[57]	CNN + GRU	1.3Ah NMC	0 °C, 10 °C, 20 °C, 26 °C, 30 °C, 40 °C and 50 °C	RMSE 4.36%, MAE 3.04% @ 0 °C
26	[58]	Autoencoder NN + LSTM	2Ah NMC [36]	Yes	RMSE 1.3%, MAE 0.93% @ 0 °C

In [57], a novel CNN-GRU network is introduced, featuring eight filters in the convolutional layer, followed by two stacked GRU layers comprising 150 and 80 nodes. The Ada-Grad optimisation algorithm is employed, updating the learning rate itself, with the initial learning rate and momentum values set to 0.001 and 0.8, respectively. All hyperparameters are determined through a trial-and-error method. Testing a 1.3Ah 18650 NMC battery cell on an Arbin BT2000 battery tester at temperatures ranging from 0 °C to 50 °C, this method achieves an RMSE of 4.36% and MAE of 3.04% at 0 °C. The proposed approach outperforms the ELM, SVM, and GRU methods while also maintaining a satisfactory SOC estimation speed, making it suitable for real-time applications. Replacing conventional matrix multiplications with convolutions within the gated recurrent unit represents a novel approach that effectively captures temporal dependencies in SOC prediction for the first time. However, the study's limitation lies in the absence of generalisation, as it solely relies on testing with a single dataset.

In [58], the authors proposed a combined method using an Autoencoder and an LSTM RNN. The Autoencoder NN with one hidden layer containing 22 neurons extracts

relevant features, which are then fed into the LSTM RNN consisting of one layer with 100 units. To address overfitting, L2 regularisation and dropout with values of 0.001 and 0.5, respectively, are implemented. Utilising a CALCE [36] dataset of a 2Ah 18650 NMC battery cell, the model achieved a 1.3% RMSE and 0.93% MAE at 0 °C. Comparative tests with a multilayer perceptron NN, having 1 hidden layer and 25 neurons, revealed that the proposed method performed better for all temperatures, including 0 °C, 25 °C, and 45 °C. Through the utilisation of an Autoencoder for optimal feature extraction and an LSTM for prediction, the authors attain commendable performance. Nevertheless, this achievement is constrained to a single dataset, and the study lacks the inclusion of multiple datasets, which is crucial for robust validation. Additionally, the absence of publicly available datasets hinders effective comparisons with other methodologies.

6. Conclusions

Recently, there has been an increase in data-driven techniques, driven by advancements in microcontrollers and the volume of available information. These data-driven estimation algorithms have shown remarkable capability in recreating equivalent models of battery cells and packs, leading to accurate SOC estimation with low errors. Among the popular techniques, RNNs have gained prominence due to their ability to capture dynamic time dependencies in battery behaviour. The effectiveness of these models is greatly impacted by a number of factors, including the input data, hyperparameters, optimisation algorithms, temperature, and neural network architecture. Often, finding the optimal parameter values requires a trial-and-error approach. Additionally, there is a need to strike a balance between the estimation time and performance, as SOC estimation is frequently required for real-time applications. Therefore, future research should focus on developing hybrid models in which machine learning methods are combined with optimisation methods to fine-tune the hyperparameters. By delving into hybrid models, researchers can further increase the overall performance of the model. Using machine learning models in conjunction with optimisation algorithms opens new avenues for enhanced battery SOC estimation techniques.

To propel the advancement of data-driven SOC estimation algorithms, several key recommendations should be considered. Incorporating key variables such as SOH, which signifies a battery's present capacity compared to its initial capacity, and RUL, denoting its projected lifespan, improves the accuracy of SOC estimations. The inclusion of SOH provides insight into the battery's current efficiency, allowing for adjustments in SOC predictions to match the diminished or retained capacity. Meanwhile, RUL offers insight into how long the battery will sustain its operations for, enabling a more informed assessment of the charge levels over its remaining lifespan. Furthermore, broadening the research scope from single cells to battery packs is crucial for practical applications. Developing a transfer model that can achieve high performance with low computational costs for various battery types is also essential. Implementing a BMS with internet connectivity to leverage cloud applications can reduce computational expenses and enable efficient data storage. Adopting more advanced techniques for the selection of hyperparameters and model parameters is advisable to attain superior performance. Furthermore, the prevailing approach for SoC estimation involves the use of physics-informed neural networks. This trend is driven by the aim to accelerate computational processes during testing, ultimately leading to reduced power consumption if the model is integrated into a real BMS. Additionally, there is the growing adoption of transformer-based algorithms in handling time series data. However, one research work demonstrates that transformer-based algorithms might not be well suited to this data type, resulting in higher error rates when compared to simple data-driven methods. Lastly, deep learning models should predict SOC values and swiftly detect battery faults, such as thermal runaways, to safeguard both the battery and human safety.

Author Contributions: P.E.: data curation, formal analysis, investigation, supervision, writing—original draft, review and editing. S.G.: data curation, formal analysis, writing—original draft.

S.L.: conceptualisation, supervision, writing—review and editing, methodology, project administration. E.O.: conceptualisation, supervision, writing—review and editing, methodology, project administration. All authors have read and agreed to the published version of the manuscript.

Nomenclature

(SOC)	State of Charge
(EOL)	End of Life
(ECM)	Equivalent Circuit Model
(PF)	Particle Filter
(KF)	Kalman Filter
(ANN)	Artificial Neural Network
(ACKF)	Adaptive Cubature Kalman Filter
(EKF)	Extended Kalman Filter
(SOH)	State of Health
(BMS)	Battery Management System
(RNN)	Recurrent Neural Network
(LSTM)	Long Short-Term Memory
(biLSTM)	Bidirectional Long Short-Term Memory
(LIBs)	Lithium-Ion Batteries
(CC)	Coulomb Counting
(UKF)	Unscented Kalman Filter
(GRU)	Gated Recurrent Unit
(biGRU)	Bidirectional Gated Recurrent Unit
(FC)	Fully Connected
(CNN-GRU)	Convolution Gated Recurrent Unit
(PSO)	Particle Swarm optimisation
(LSA)	Lighting Search Algorithm
(GA)	Genetic Algorithm
(NARX)	Nonlinear Autoregresive with Exogenous Input
(GM)	Grey Model
(SGAGM)	Sliding Genetic Algorithm Grey Model
(LS-SVM)	Least-Square Support Vector Machine
(NMC)	Nickel Manganese Cobalt Oxide
(LFP)	Lithium Iron Phosphate
(MAE)	Mean Absolute Error
(UPF)	Unscented Particle Filter
(LCO)	Lithium Cobalt Oxide
(RMSE)	Root Mean Squared Error
(CALCE)	Centre for Advanced Life Cycle Engineering
(UDDS)	Urban Dynamometer Driving Schedule
(HWFET)	Highway Fuel Economy Test Cycle
(US06)	Highway Driving Schedule
(LA92)	California Unified Cycle
(DST)	Dynamic Stress Test
(FUDS)	Federal Urban Drive Schedule

(BJDST)	Beijing Dynamic Stress Test
(SVM)	Support Vector Machine
(GPR)	Gaussian Process Regression
(FFNN)	Feedforward Neural Network
(NCA)	Nickel Cobalt Aluminum Oxide
(DNN)	Deep Neural Network
(TCN)	Temporal Convolutional Network
(BSA)	Backtracking Search Algorithm
(GSA)	Gravitational Search Algorithm
(ELM)	Extreme Learning Machine
(BPNN)	Backpropagation Neural Network
(RBFNN)	Radial Basis Function Neural Network
(GRNN)	Generalised Regression Neural Network
(DBN)	Deep Belief Network
(RNARX)	Recurrent Nonlinear Autoregressive with Exogenous Inputs
(SGAGM)	Sliding Genetic Algorithm Grey Model
(GM)	Grey Model

References

1. Yong, J.Y.; Ramachandaramurthy, V.K.; Tan, K.M.; Mithulananthan, N. A review on the state-of-the-art technologies of electric vehicle, its impacts and prospects. *Renew. Sustain. Energy Rev.* **2015**, *49*, 365–385. [CrossRef]
2. Forbes: How Renewables Could Kill off Fossil Fuel Electricity by 2035: New Report. Available online: https://www.forbes.com/sites/davidrvetter/2021/04/26/how-renewables-could-kill-off-fossil-fuel-electricity-by-2035-new-report/?sh=56f63a5565ed/ (accessed on 13 June 2023).
3. Blomgren, G.E. The development and future of lithium ion batteries. *J. Electrochem. Soc.* **2016**, *164*, A5019–A5025. [CrossRef]
4. Eleftheriadis, P.; Leva, S.; Gangi, M.; Rey, A.V.; Borgo, A.; Coslop, G.; Groppo, E.; Grande, L.; Sedzik, M. Second life batteries: Current regulatory framework, evaluation methods and economic assessment. In Proceedings of the 2022 IEEE International Conference on Environment and Electrical Engineering and 2022 IEEE Industrial and Commercial Power Systems Europe (EEEIC/I CPS Europe), Prague, Czech Republic, 28 June–1 July 2022.
5. Rahimi-Eichi, H.; Ojha, U.; Baronti, F.; Chow, M.-Y. Battery management system: An overview of its application in the smart grid and electric vehicles. *IEEE Ind. Electron. Mag.* **2013**, *7*, 4–16. [CrossRef]
6. Eleftheriadis, P.; Leva, S.; Gangi, M.; Rey, A.V.; Groppo, E.; Grande, L. Comparative study of machine learning techniques for the state of health estimation of li-ion batteries. In Proceedings of the 13th Mediterranean Conference on Power Generation, Transmission, Distribution and Energy Conversion (MEDPOWER2022), Valletta, Malta, 7–9 November 2022; pp. 1–6.
7. Pop, V.; Bergveld, H.J.; Notten, P.H.L.; Regtien, P.P. State-of-the-art of battery state-of-charge determination. *Meas. Sci. Technol.* **2005**, *16*, R93. [CrossRef]
8. Petropoulos, F. Others Forecasting: Theory and practice. *Int. J. Forecast.* **2022**, *38*, 705–871. [CrossRef]
9. Snihir, I.; Rey, W.; Verbitskiy, E.; Belfadhel-Ayeb, A.; Notten, P.H. Battery open-circuit voltage estimation by a method of statistical analysis. *J. Power Sources* **2006**, *159*, 1484–1487. [CrossRef]
10. Ng, K.S.; Moo, C.S.; Chen, Y.P.; Hsieh, Y.C. Enhanced coulomb counting method for estimating state-of-charge and state-of-health of lithium-ion batteries. *Appl. Energy* **2009**, *86*, 1506–1511. [CrossRef]
11. Xiong, R.; Tian, J.; Shen, W.; Sun, F. A novel fractional order model for state of charge estimation in lithium ion batteries. *IEEE Trans. Veh. Technol.* **2018**, *68*, 4130–4139. [CrossRef]
12. Chen, Z.; Sun, H.; Dong, G.; Wei, J.; Wu, J.I. Particle filter-based state-of-charge estimation and remaining-dischargeable-time prediction method for lithium-ion batteries. *J. Power Sources* **2019**, *414*, 158–166. [CrossRef]
13. Zhang, Y.; Xiong, R.; He, H.; Shen, W. Lithium-ion battery pack state of charge and state of energy estimation algorithms using a hardware-in-the-loop validation. *IEEE Trans. Power Electron.* **2016**, *32*, 4421–4431. [CrossRef]
14. Zhong, Q.; Zhong, F.; Cheng, J.; Li, H.; Zhong, S. State of charge estimation of lithium-ion batteries using fractional order sliding mode observer. *ISA Trans.* **2017**, *66*, 448–459. [CrossRef] [PubMed]
15. Lipu, M.; Hannan, M.; Hussain, A.; Ayob, A.; Saad, M.H.; Karim, T.F.; How, D.N. Data-driven state of charge estimation of lithium-ion batteries: Algorithms, implementation factors, limitations and future trends. *J. Clean. Prod.* **2020**, *277*, 124110. [CrossRef]
16. Hannan, M.; Lipu, M.; Hussain, A.; Mohamed, A. A review of lithium-ion battery state of charge estimation and management system in electric vehicle applications: Challenges and recommendations. *Renew. Sustain. Energy Rev.* **2017**, *78*, 834–854. [CrossRef]
17. Xiong, R.; Cao, J.; Yu, Q.; He, H.; Sun, F. Critical review on the battery state of charge estimation methods for electric vehicles. *IEEE Access* **2018**, *6*, 1832–1843. [CrossRef]
18. How, D.N.T.; Hannan, M.A.; Lipu, M.S.H.; Ker, P.J. State of charge estimation for lithium-ion batteries using model-based and data-driven methods: A review. *IEEE Access* **2019**, *7*, 136116–136136. [CrossRef]

19. Wang, Y.; Tian, J.; Sun, Z.; Wang, L.; Xu, R.; Li, M.; Chen, Z. A comprehensive review of battery modeling and state estimation approaches for advanced battery management systems. *Renew. Sustain. Energy Rev.* **2020**, *131*, 110015. [CrossRef]
20. Vidal, C.; Malysz, P.; Kollmeyer, P.; Emadi, A. Machine learning applied to electrified vehicle battery state of charge and state of health estimation: State-of-the-art. *IEEE Access* **2020**, *8*, 52796–52814. [CrossRef]
21. Cui, Z.; Wang, L.; Li, Q.; Wang, K. A comprehensive review on the state of charge estimation for lithium-ion battery based on neural network. *Int. J. Energy Res.* **2022**, *46*, 5423–5440. [CrossRef]
22. Cervantes, J.; Garcia-Lamont, F.; Rodríguez-Mazahua, L.; Lopez, A. A comprehensive survey on support vector machine classification: Applications, challenges and trends. *Neurocomputing* **2020**, *408*, 189–215. [CrossRef]
23. Gokmen, Z.; Elmali, F.; Ozturk, A. Bagging support vector machines for leukemia classification. *Int. J. Comput. Sci. Issues (IJCSI)* **2012**, *9*, 355.
24. Song, Y.; Liu, D.; Liao, H.; Peng, Y. A hybrid statistical data-driven method for on-line joint state estimation of lithium-ion batteries. *Appl. Energy* **2020**, *261*, 114408. [CrossRef]
25. Eric, S.; Speekenbrink, M.; Krause, A. A tutorial on Gaussian process regression with a focus on exploration-exploitation scenarios. *BioRxiv* **2017**. [CrossRef]
26. Deng, Z.; Hu, X.; Lin, X.; Che, Y.; Xu, L.; Guo, W. Data-driven state of charge estimation for lithium-ion battery packs based on gaussian process regression. *Energy* **2020**, *205*, 118000. [CrossRef]
27. Chen, X.; Chen, X.; Chen, X. A novel framework for lithium-ion battery state of charge estimation based on kalman filter gaussian process regression. *Int. J. Energy Res.* **2021**, *5*, 13238–13249. [CrossRef]
28. Chen, C.; Xiong, R.; Yang, R.; Shen, W.; Sun, F. State-of-charge estimation of lithium-ion battery using an improved neural network model and extended kalman filter. *J. Clean. Prod.* **2019**, *234*, 1153–1164. [CrossRef]
29. Chemali, E.; Kollmeyer, P.J.; Preindl, M.; Emadi, A. State-of-charge estimation of li-ion batteries using deep neural networks: A machine learning approach. *J. Power Sources* **2018**, *400*, 242–255. [CrossRef]
30. Liu, Y.; Li, J.; Zhang, G.; Hua, B.; Xiong, N. State of charge estimation of lithium-ion batteries based on temporal convolutional network and transfer learning. *IEEE Access* **2021**, *9*, 34177–34187. [CrossRef]
31. Meriem, B.; Batouche, M. Deep learning for ligand-based virtual screening in drug discovery. In Proceedings of the 2018 3rd International Conference on Pattern Analysis and Intelligent Systems (PAIS), Tebessa, Algeria, 24–25 September 2018.
32. Bednarski, B.P.; Singh, A.D.; Zhang, W.; Jones, W.M.; Ramezani, A.N.R. Temporal convolutional networks and data rebalancing for clinical length of stay and mortality prediction. *Sci. Rep.* **2022**, *12*, 21247. [CrossRef]
33. Chemali, E.; Kollmeyer, P.J.; Preindl, M.; Ahmed, R.; Emadi, A. Long short-term memory networks for accurate state-of-charge estimation of li-ion batteries. *IEEE Trans. Ind. Electron.* **2018**, *65*, 6730–6739. [CrossRef]
34. Yang, F.; Song, X.; Xu, F.; Tsui, K.-L. State-of-charge estimation of lithium-ion batteries via long short-term memory network. *IEEE Access* **2019**, *7*, 53792–53799. [CrossRef]
35. Tian, Y.; Lai, R.; Li, X.; Xiang, L.; Tian, J. A combined method for state-of-charge estimation for lithium-ion batteries using a long short-term memory network and an adaptive cubature kalman filter. *Appl. Energy* **2020**, *265*, 114789. [CrossRef]
36. Calce. lithium-Ion Battery Experimental Data. Available online: https://web.calce.umd.edu/batteries/data.htm (accessed on 13 June 2023).
37. Yang, F.; Zhang, S.; Li, W.; Miao, Q. State-of-charge estimation of lithium-ion batteries using lstm and ukf. *Energy* **2020**, *201*, 117664. [CrossRef]
38. Mamo, T.; Wang, F.-K. Long short-term memory with attention mechanism for state of charge estimation of lithium-ion batteries. *IEEE Access* **2020**, *8*, 94140–94151. [CrossRef]
39. Kollmeyer, P. Panasonic 18650pf li-ion battery data. *Mendeley Data* **2018**, *1*. [CrossRef]
40. Bian, C.; He, H.; Yang, S. Stacked bidirectional long short-term memory networks for state-of-charge estimation of lithium-ion batteries. *Energy* **2020**, *191*, 116538. [CrossRef]
41. Bian, C.; He, H.; Yang, S.; Huang, T. State-of-charge sequence estimation of lithium-ion battery based on bidirectional long short-term memory encoder-decoder architecture. *J. Power Sources* **2020**, *449*, 227558. [CrossRef]
42. Yang, F.; Li, W.; Li, C.; Miao, Q. State-of-charge estimation of lithium-ion batteries based on gated recurrent neural network. *Energy* **2019**, *175*, 66–75. [CrossRef]
43. Li, C.; Xiao, F.; Fan, Y. An approach to state of charge estimation of lithium-ion batteries based on recurrent neural networks with gated recurrent unit. *Energies* **2019**, *12*, 1592. [CrossRef]
44. Jiao, M.; Wang, D.; Qiu, J. A gru-rnn based momentum optimised algorithm for soc estimation. *J. Power Sources* **2020**, *459*, 228051. [CrossRef]
45. Xiao, B.; Liu, Y.; Xiao, B. Accurate state-of-charge estimation approach for lithium-ion batteries by gated recurrent unit with ensemble optimiser. *IEEE Access* **2019**, *7*, 54192–54202. [CrossRef]
46. Lipu, M.S.H.; Hannan, M.A.; Hussain, A.; Saad, M.H.; Ayob, A.; Uddin, M.N. Extreme learning machine model for state-of-charge estimation of lithium-ion battery using gravitational search algorithm. *IEEE Trans. Ind. Appl.* **2019**, *55*, 4225–4234. [CrossRef]
47. Hannan, M.A.; Lipu, M.S.H.; Hussain, A.; Saad, M.H.; Ayob, A. Neural network approach for estimating state of charge of lithium-ion battery using backtracking search algorithm. *IEEE Access* **2018**, *6*, 10069–10079. [CrossRef]
48. Liu, D.; Li, L.; Song, Y.; Wu, L.; Peng, Y. Hybrid state of charge estimation for lithium-ion battery under dynamic operating conditions. *Int. J. Electr. Power Energy Syst.* **2019**, *110*, 48–61. [CrossRef]

49. Bole, B.; Kulkarni, C.; Daigle, M. Randomized Battery Usage Data Set. 2014. Available online: https://ti.arc.nasa.gov/tech/dash/groups/pcoe/prognostic-data-repository/ (accessed on 13 June 2023).

50. Guo, Y.; Yang, Z.; Liu, K.; Zhang, Y.; Feng, W. A compact and optimised neural network approach for battery state-of-charge estimation of energy storage system. *Energy* **2021**, *219*, 119529. [CrossRef]

51. Hannan, M.A.; Lipu, M.S.H.; Hussain, A.; Ker, P.J.; Mahlia, T.M.I.; Mansor, M.; Ayob, A.; Saad, M.H.; Dong, Z.Y. Toward enhanced state of charge estimation of lithium-ion batteries using optimised machine learning techniques. *Sci. Rep.* **2020**, *10*, 4687. [CrossRef] [PubMed]

52. Lipu, M.S.H.; Hannan, M.A.; Hussain, A.; Saad, M.H.M.; Ayob, A.; Blaabjerg, F. State of charge estimation for lithium-ion battery using recurrent narx neural network model based lighting search algorithm. *IEEE Access* **2018**, *6*, 28150–28161. [CrossRef]

53. Chen, L.; Wang, Z.; Lü, Z.; Li, J.; Ji, B.; Wei, H.; Pan, H. A novel state-of-charge estimation method of lithium-ion batteries combining the grey model and genetic algorithms. *IEEE Trans. Power Electron.* **2018**, *33*, 8797–8807. [CrossRef]

54. Saha, B.; Goebel, K. Uncertainty management for diagnostics and prognostics of batteries using bayesian techniques. In Proceedings of the 2008 IEEE Aerospace Conference, Big Sky, MT, USA, 1–8 March 2008; pp. 1–8.

55. Song, X.; Yang, F.; Wang, D.; Tsui, K.-L. Combined cnn-lstm network for state-of-charge estimation of lithium-ion batteries. *IEEE Access* **2019**, *7*, 88894–88902. [CrossRef]

56. Wei, M.; Ye, M.; Li, J.B.; Wang, Q.; Xu, X. State of charge estimation of lithium-ion batteries using lstm and narx neural networks. *IEEE Access* **2020**, *8*, 189236–189245. [CrossRef]

57. Huang, Z.; Yang, F.; Xu, F.; Song, X.; Tsui, K.-L. Convolutional gated recurrent unit–recurrent neural network for state-of-charge estimation of lithium-ion batteries. *IEEE Access* **2019**, *7*, 93139–93149. [CrossRef]

58. Fasahat, M.; Manthouri, M. State of charge estimation of lithium-ion batteries using hybrid autoencoder and long short term memory neural networks. *J. Power Sources* **2020**, *469*, 228375. [CrossRef]